photonics

MDPI

Article

Investigation of Side Wall Roughness Effect on Optical Losses in a Multimode Si_3N_4 Waveguide Formed on a Quartz Substrate

Anastasia Yakuhina *, Alexey Kadochkin, Vyacheslav Svetukhin, Dmitry Gorelov, Sergey Generalov and Vladimir Amelichev

Scientific-Manufacturing Complex Technological Centre, Zelenograd, Moscow 124498, Russia; askadochkin@sv.ulsu.ru (A.K.); V.Svetukhin@tcen.ru (V.S.); D.Gorelov@tcen.ru (D.G.); S.Generalov@tcen.ru (S.G.); V.Amelichev@tcen.ru (V.A.)

* Correspondence: A.Yakuhina@tcen.ru; Tel.: +7-499-720-8779

Received: 25 September 2020; Accepted: 5 November 2020; Published: 7 November 2020

Abstract: This article presents the results of the study of the influence of the most significant parameters of the side wall roughness of an ultra-thin silicon nitride lightguide layer of multimode integrated optical waveguides with widths of 3 and 8 microns. The choice of the waveguide width was made due to the need to provide multimode operation for telecommunication wavelengths, which is necessary to ensure high integration density. Scattering in waveguide structures was measured by optical frequency domain reflectometry (OFDR) of a backscattering reflectometer. The finite difference time domain method (FDTD) was used to study the effect of roughness parameters on optical losses in fabricated waveguides, the roughness parameters that most strongly affect optical scattering were determined, and methods of its significant reduction were specified. The prospects for implementing such structures on a quartz substrate are justified.

Keywords: integrated optics; silicon technology; silicon nitride; photonics; reflectometry; attenuation; integrated optical waveguide structure; multimode integrated optical waveguide; optical loss; roughness

1. Introduction

Silicon photonics, which is a synergy of two groups of technologies—optics and electronics—is among the most well-known technological platforms for implementing photonic integrated circuits today [1]. Among the main advantages of such circuits is compatibility with standard silicon technologies. This makes it possible to manufacture silicon photonics devices using standard technological processes using existing production lines used for the production of electronic integrated circuits. This method allows the possible financial costs caused by the launch of specialized production to be minimized [2].

Recently, multimode photonics has attracted increasing attention; the introduction of higher-level modes allows an increase in the number of channels for data transmission in systems with mode-division-multiplexed systems (MDM). Multimode waveguides involve not only the fundamental mode but also higher-level modes. The mode dispersion in a multimode integrated optical waveguide is extremely large. This allows efficient mode manipulation to be realized—among the most important properties for multimode integrated photonics [3]. Most integrated photonics devices are designed on the basis of single-mode integrated optical waveguide structures, since higher-level modes cause crosstalk and losses because of multimode interference (MMI) [4,5]. However, the technology based on MMI allows the implementation of highly sensitive temperature sensors [6], chemical sensors, biosensors [7,8], which have many advantages, such as ease of operation and high sensitivity [9].

One of the ways to implement integrated optical waveguide structures is based on SOI-technology (silicon on insulator) assuming the use of silicon as a waveguide layer and silicon oxide as a cladding [10,11]. Interest in this method of implementation consisted mainly of the high contrast index for a silicon waveguide with a silicon oxide cladding (n_{Si} = 3.46 vs. n_{SiO2} = 1.46) and CMOS (complementary metal-oxide-semiconductor) compatibility. However, although such a high contrast index makes it possible to implement a unique function on a very compact area, it leads to significant internal losses in the material of the lightguide layer, which is associated with the intrinsic structural features of the silicon crystal (scattering of radiation by free carriers in silicon) [2,12]. So, the implementation of photonic integrated circuits (PIC) based on such waveguides is extremely inefficient.

Thus, there is an interest in exploring alternative material combinations that meet the same requirements. Previously, asymmetrical waveguide structures using a covering layer made of tellurium oxide were considered [13,14]. We draw our attention in this work to symmetrical waveguides, demonstrating better localization of guided mode in Si_3N_4 waveguide core with the waveguide cladding made of SiO_2 [15–17]. Such waveguide structures have a number of undeniable advantages. First, a moderately high contrast index (n_{Si3N4} = 2.0 vs. n_{SiO2} = 1.46) reduces the impact of manufacturing defects on the devices [2]. Second, the negligible two-photon scattering inherent of silicon nitride in the near-infrared region of the spectrum allows waveguide structures with low optical losses, as well as resonators with high Q-factors to be demonstrated [18–21]. Finally, due to the promising nonlinear properties of silicon nitride waveguides and wide transparency window spanning from visible to far-infrared spectra, they benefit from parametric amplification [22–25], soliton microcomb [26], broadband supercontinuum generation [27], etc. Thus, the use of such waveguide structures opens up a wide range of new possibilities for CMOS-compatible integrated photonics [17]. In particular, this technology can be an optimal solution for manufacturing biosensors in the visible and near-infrared ranges [28–30], where low losses and low sensitivity to thermal changes have a crucial role. In addition, it also benefits gas sensors, which are critical for a variety of applications, including medical diagnostics, pollution monitoring, and quality control of the manufacturing process [31,32].

In the manufacture of waveguide structures from silicon nitride, there are a number of problems preventing their effective use for the applications described above. One such problem is the roughness of the edge of the lightguide layer from both silicon and silicon nitride. Ways to solve this problem have previously been the subject of special attention [33–35]. In our article, we propose a method for identifying the most significant parameters of the side wall roughness of an ultra-thin silicon nitride lightguide layer in terms of the degree of their effect on optical losses in the waveguide structure. We show that changing these parameters also changes the value of optical loss. This leads to the conclusion of which specific technological operations should be optimized during the manufacturing. In addition, following the path of reducing optical losses, we propose a way to implement such waveguide structures based on a quartz substrate, citing the justification of the undeniable advantages of using such a material system while maintaining the possibility of their manufacture within existing CMOS-productions sites.

2. Fabrication

When choosing the geometric parameters of the studied waveguides, we were guided by the possibility of implementing such structures in standard silicon technologies. The width of the lightguide layer was chosen in such a way that the formed waveguide supports a multimode mode of operation for telecommunications wavelengths (1.55 microns), and also meets the condition to provide a high density of integration of devices that are planned to be manufactured on their basis in the future. We chose the thickness of the lightguide layer made of silicon nitride to be 200 nm, which ensures a strong interaction of the field with the upper cladding and a high level of integration [28–30,36]. When creating waveguide structures, we used bilaterally polished semiconductor quartz wafers with a surface roughness (Ra): <0.5 nm, in contrast to the standard approach implying the use of a silicon

substrate followed by the formation of a lower cladding from thermal oxide [36]. Such a low surface roughness of the wafer allows us to form subsequent layers of the waveguide structure with minimal roughness. This makes the upper and lower interfaces almost perfect, so scattering at these interfaces can be neglected. In addition, the use of a quartz wafer as a substrate allows formation of a silicon nitride waveguiding layer to begin immediately. It reduces the possibility of introducing additional defects at the production stages, as well as the cost and production time significantly. Additionally, this way of implementing waveguide structures is fully compatible with silicon technology.

When using silicon wafers as a substrate, there is always a risk of guided wave leakage into the substrate. This is due to the fact that (as mentioned earlier) the contrast index in the Si-SiO_2 structure is significantly higher than the contrast index of the Si_3N_4—SiO_2 structure [2]. In this case, the slightest error in choosing the thickness of the lower cladding of the waveguide structure made of thermal oxide, as well as with minimal deviations of the angle at which the radiation enters the device, significantly increases the risk of radiation leakage into the substrate. The use of quartz wafers instead of silicon ones completely eliminates the possibility of such leakage due to difference in contrast indices and allows a reduction in entering losses of the optical device.

Figure 1 shows a diagram of the route for fabricating silicon nitride waveguide structures on a quartz substrate. At the first stage, a 200-nm-thick Low-pressure Chemical Vapor Deposition (LPCVD) layer of silicon nitride was formed on a quartz substrate. Precipitation was carried out using a precursor consisting of a mixture of gaseous dichlorsilane (DCS) (SiH_2Cl_2) and ammonia (NH_3). LPCVD nitride was chosen for its better uniformity and thickness due to the fact that lowered pressure reduces the probability of undesirable reactions in the gas phase and leads to more uniform deposition of the film on the substrate [37,38]. The refractive index of the film obtained was investigated by spectral ellipsometry and is equal to n = 2.0. Comparative characteristics of silicon, nitride and silicon oxide are shown in Table 1.

At the next stage, a waveguide layer of silicon nitride was formed using photolithography and plasma-chemical etching of Si_3N_4.

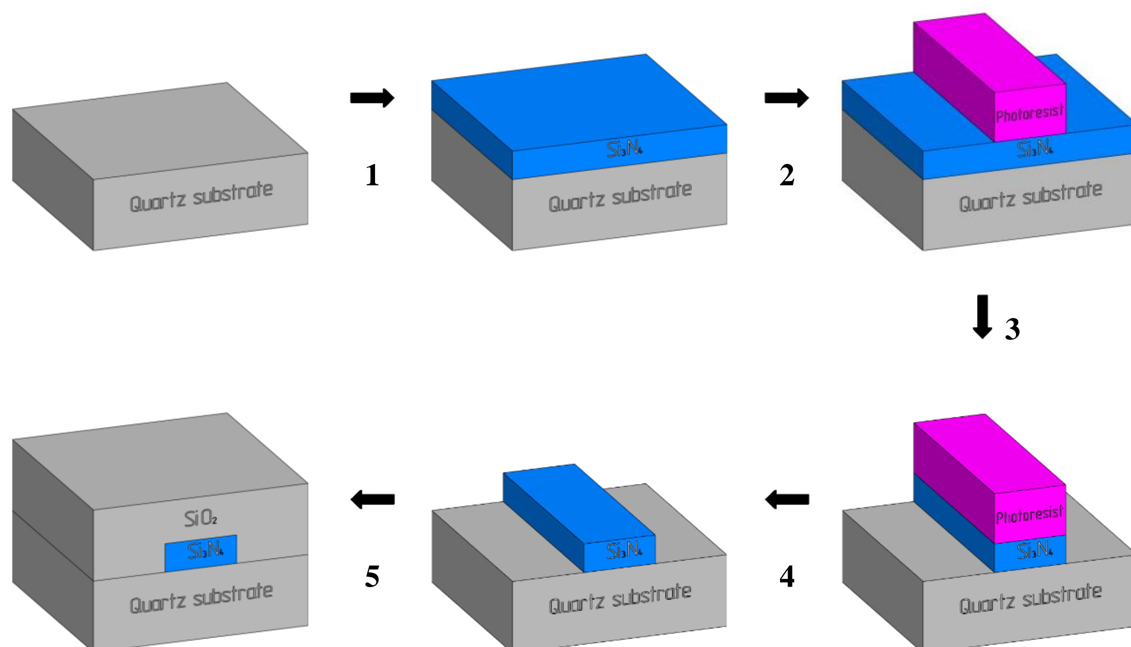

Figure 1. The fabrication steps for the integration waveguide with core Si_3N_4 based quartz substrate: 1—core deposition Si_3N_4 (LPCVD, 790 °C); 2—spin photoresist, UV exposure and developed; 3—plasma etch (core etch) Si_3N_4; 4—remove photoresist; 5—upper cladding deposition using TEOS (tetraethyl orthosilicate)-based PECVD (plasma enhanced chemical vapor deposition).

Table 1. Comparison of silicon, silicon nitride and silicon oxide, information extracted from LIGENTEC [39].

	Silicon	Silicon Nitride	Silicon Oxide
Transparency	1.1–9 μm	0.25–8 μm	0.13–3.5 μm
Band gap	1.12 eV	5 eV	9 eV
Refractive index at 1550 nm	3.8	2.00	1.46
Nonlinear coefficient (m^2W^{-1})	$\approx 6 \times 10^{-18}$	$\approx 2 \times 10^{-19}$	$\approx 2.5 \times 10^{-20}$
Deposition	Crystal EPI/SOI	LPCVD	Thermal oxide

After the formation of the waveguide layer, the roughness of its side walls was studied. The roughness measurement of the silicon nitride waveguide samples was performed by analyzing the side wall roughness of identical control silicon waveguide formed in the same technological process as the silicon nitride ones using a (SEM). This method of estimation was chosen due to the fact that when studying fully dielectric structures, which the waveguide structures we describe made on quartz substrates are, a charge accumulates in the dielectric layers in a scanning electron microscope, which causes the frame to "light up" and hinders the analysis. Performing the analysis on similar control structures made on a silicon substrate reduces the effect of charge accumulation due to the "flow" of charge into silicon. As a result, it was found that the roughness of the side wall of the silicon nitride etching profile has a wavelike shape with a period of about 30–33 nm and a deviation of the edge from the vertical plane to 64 nm (Figure 2).

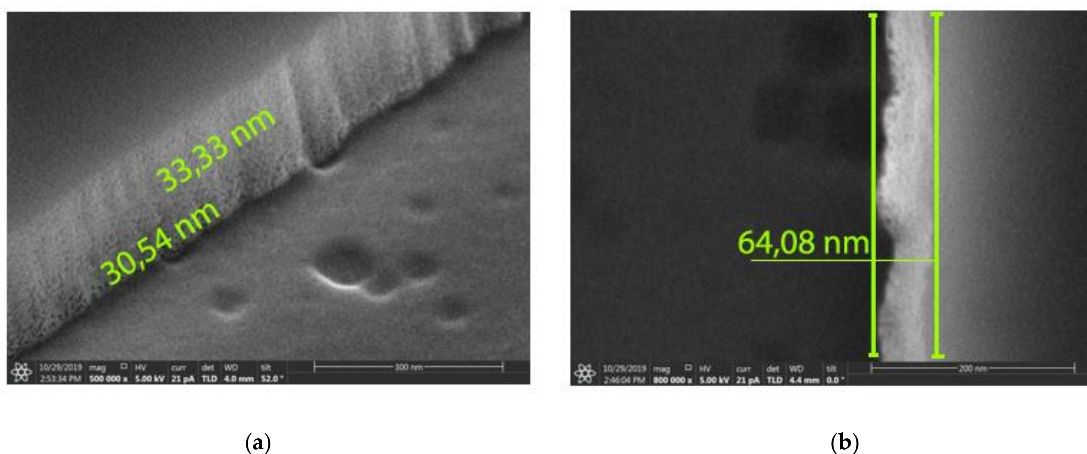

(**a**) (**b**)

Figure 2. SEM image of the side surface of the silicon nitride profile after plasma-chemical etching: side view (**a**); view from above (**b**).

Then, the upper layer of the waveguide structure was formed by deposition of the silicon oxide film. The refractive index of this silicon oxide film was also studied by spectral ellipsometry and was defined to be 1.46, which is as close as possible to the refractive index of the quartz substrate. This allows us to conclude that the resulting waveguide structure is as close to symmetric as possible.

3. Study of Fabricated Waveguides

Optical loss was estimated using optical frequency domain reflectometry (OFDR) in optical backscatter reflectometer (OBR). OFDR is an interferometric measurement technique that uses a highly coherent, continuously tunable laser light source. The analysis of the interference pattern is carried out using the Fourier transform that makes it possible to obtain the dependence of the reflection intensity on the distance to the point of introduction of the probe radiation. This method is optimal for solving problems that require a combination of high speed, sensitivity and resolution in the analysis of short and intermediate transmission line lengths [40,41]. Figure 3 shows a scheme of studying optical losses for fabricated waveguide samples.

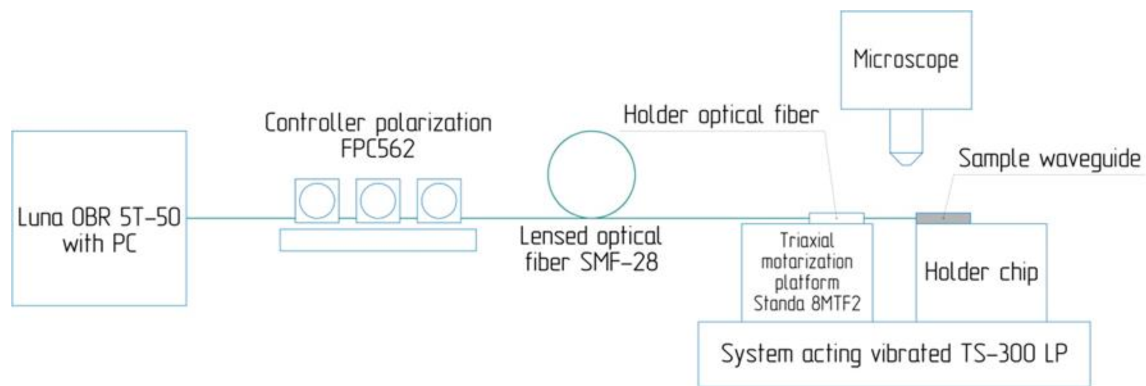

Figure 3. Scheme of studying optical losses in waveguides with widths of 3 and 8 microns.

Figure 4 shows a reflectogram of the test waveguide structure with a width of 8 microns and a length of 60 mm, which has the lowest optical losses. Table 2 shows the results of the study of waveguides that were also made in this research. The waveguide parameters were measured using a Luna OBR 5T-50 optical backscattering reflectometer connected through the FPC562 fiber polarization controller (FPC). Optical radiation entered the waveguide using an SMF-28 lensed fiber. FPC was used to adjust the polarization of light, since the optical radiation coming out of the reflectometer has an arbitrary form of polarization (a common case of polarization is elliptical type of polarization of light). Monitoring of changes in polarization was made by the response of the reflectogram. Horizontal linear polarization corresponds to minimal optical losses— i.e., the minimum slope of the reflectogram (Figure 4a), which is also associated with a high aspect ratio of the waveguide. Due to the sufficient noise level of the obtained reflectograms (Figure 4a), as well as in order to obtain more reliable values of optical losses in the waveguide, linear extrapolation was performed (Figure 4b). Additionally, dead zones for events, such as reflections from the crystal ends at the input and output of the waveguide, were excluded.

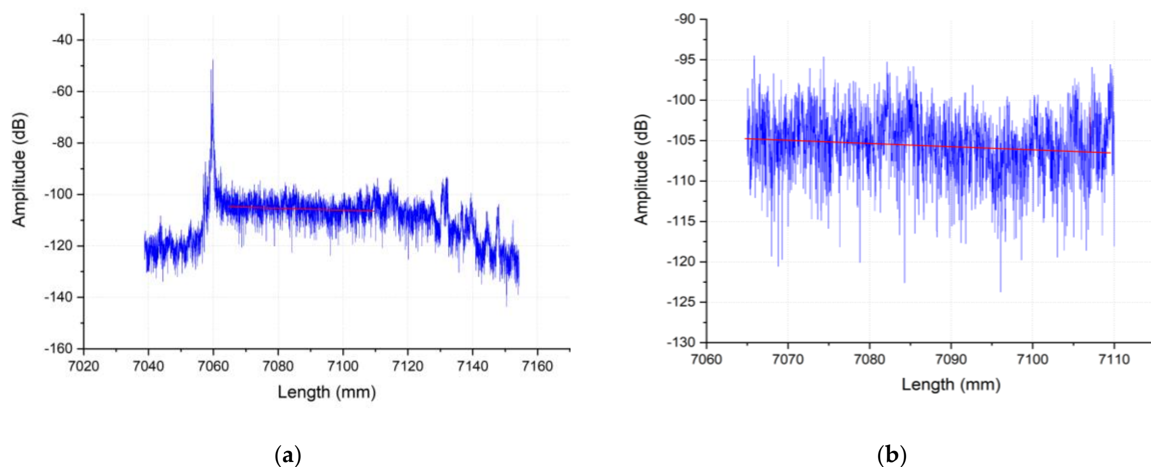

Figure 4. Waveguide reflectogram with a width of 8 microns and a length of 60 mm: general view (**a**); section with linear extrapolation (**b**).

Table 2. Optical losses for waveguide structures with widths of 3 and 8 microns and a length of 60 mm.

Waveguide Structure Width, μm	Optical Loss, dB/cm
3	1.43
8	0.31

4. Calculation of the Influence of the Side Walls' Roughness of a Silicon Nitride Layer on Optical Losses in the Waveguide

To calculate the effect of the roughness of the side walls of a silicon nitride lightguide layer on optical losses in a multimode optical waveguide, a finite-difference time-domain (FDTD) method was used. The data obtained during the study of the roughness of the lightguide layer of previously manufactured waveguides were used as a basis. The σ (mean square deviation of roughness) and δ (longitudinal size of roughness) parameters used to calculate are clearly represented in Figure 5

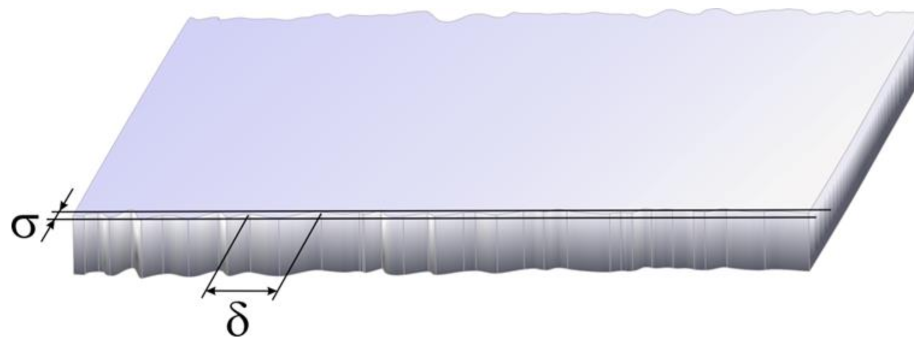

Figure 5. Schematic of the waveguide with "rough"side wall.

The roughness on side walls of the waveguide was set as a random variable with a standard deviation and a longitudinal roughness size. The results of calculations for waveguides with widths of 3 and 8 microns are shown in Table 3 and Figure 6. Figure 6 shows that when the waveguide is wider, the field strength on its side walls is less. That means better localization of energy in the center of the waveguide, and leads to significantly less attenuation on the roughness of the side walls (Table 3).

Table 3. Comparison of the measured and calculated attenuation of the TE00 mode in silicon nitride waveguides; σ—mean square deviation of roughness; δ—longitudinal size of roughness.

Waveguide Structure Width, µm	Optical Loss (Measured), dB/cm	σ, nm	δ, nm	Optical Loss (Calculated), dB/cm
3.00	1.43	30.00	20.00	1.63
		30.00	60.00	1.27
		10.00	20.00	0.22
8.00	0.31	30.00	20.00	0.11
		30.00	60.00	0.05
		10.00	20.00	0.01

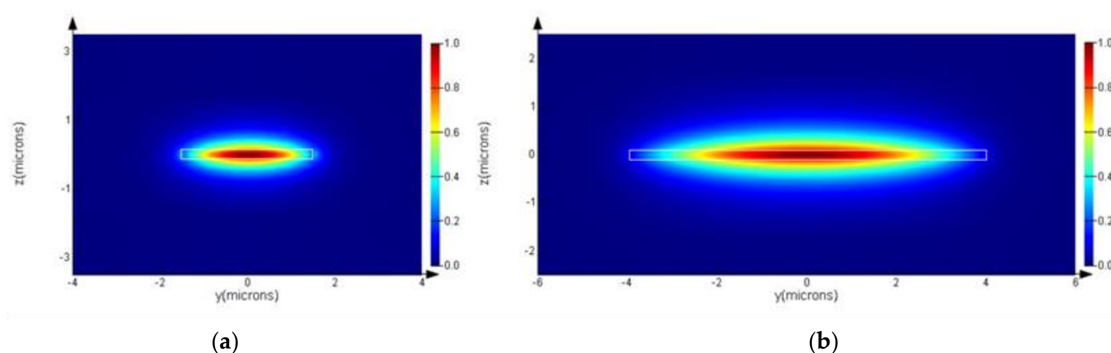

(**a**) (**b**)

Figure 6. Allocation of the normalized amplitude of electric field (mode TE00) in waveguides of various widths for a waveguide with widths of 3 (**a**) and 8 µm (**b**).

Table 3 shows that for waveguides with widths of 3 and 8 microns, reducing the roughness height by three times leads to a decrease in attenuation by an order of magnitude. The study of silicon

nitride waveguide's profile structure SEM images revealed that there is a significant variation in the longitudinal size of the roughness. Regarding this, calculations were also performed for various longitudinal roughness sizes. It can be seen (Table 3) that an increase in the longitudinal size of the roughness with a constant transverse size leads to a certain decrease in attenuation, but this parameter affects the attenuation significantly less than the transverse size. Apparently, some averaged longitudinal roughness sizes can be used for numerical estimates in this case.

5. Conclusions

Based on the data obtained, it was found that the optical losses for a waveguide with widths of 3 and 8 μm were 1.43 and 0.31 dB/cm, respectively. Loss values are consistent with the values of analogs [42–44]. Losses in a waveguide with a width 8 μm are minimal, since the intensity of the mode field at the ends is much lower than in a 3 μm wide waveguide with the same thickness. The calculation of the effect of the roughness of the side walls of the lightguide layer made of silicon nitride is sufficiently consistent with the data obtained experimentally. Based on this, we can conclude that the value of the optical loss in the waveguide is significantly affected by the transverse size of the waveguide-layer's side wall roughness. This means that to improve the surface quality of multimode integrated optical waveguides it is necessary to improve methods for forming the lightguide layer. To calculate the effect of the roughness of the side walls of a silicon nitride lightguide layer on optical losses in a multimode integrated optical waveguide, a finite-difference time-domain (FDTD) method was used. The data obtained during the study of the roughness of the lightguide layer of previously manufactured waveguides were used as a basis.

Author Contributions: Conceptualization, A.Y. and V.S.; methodology, A.Y. and A.K.; software, A.K.; validation, V.A. and S.G.; formal analysis, A.Y. and A.K.; investigation, A.Y.; resources, V.A. and V.S.; data curation, V.A., V.S. and S.G.; writing—original draft preparation, A.Y.; writing—review and editing, D.G.; visualization, A.Y. and D.G.; supervision, V.A. and S.G.; project administration, V.A. and V.S.; funding acquisition, V.A. and S.G. All authors have read and agreed to the published version of the manuscript.

Funding: This article was prepared with the financial support of the Ministry of Education and Science of the Russian Federation as part of the State Assignment for 2019 (project No. 0N59-2019-0020) "Theoretical and experimental studies of structural and technological methods for creating integrated optics elements compatible with silicon technology". The etching process was carried out using equipment "Functional control and diagnostics of micro- and nanosystem technology" on the basis of SMC "Technological centre".

Acknowledgments: This work was supported by Theoretical and experimental studies of structural and technological methods for creating integrated optics elements compatible with silicon technology. The etching process was carried out using equipment "Functional control and diagnostics of micro- and nanosystem technology" on the basis of SMC "Technological centre".

Conflicts of Interest: The authors declare no conflict of interest.

References

1. Doerr, C.R. Silicon photonic integration in telecommunications. *Front. Phys.* **2015**, *3*, 37. [CrossRef]
2. Baets, R.G.F.; Subramanian, A.Z.; Clemmen, S.; Kuyken, B.; Bienstman, P.; Le Thomas, N.; Roelkens, G.; Van Thourhout, D.; Helin, P.; Severi, S. Silicon Photonics: Silicon nitride versus silicon-on-insulator. In Proceedings of the Optical Fiber Communication Conference, Anaheim, CA, USA, 20–22 March 2016; The Optical Society: Washington, DC, USA, 2016; p. Th3J.1.
3. Li, C.; Liu, D.; Dai, D. Multimode silicon photonics. *Nanophotonics* **2018**, *8*, 227–247. [CrossRef]
4. Streshinsky, M.; Ding, R.; Liu, Y.; Novack, A.; Galland, C.; Lim, A.E.-J.; Lo, P.G.-Q.; Baehr-Jones, T.; Hochberg, M. The Road to Affordable, Large-Scale Silicon Photonics. *Opt. Photonics News* **2013**, *24*, 32–39. [CrossRef]
5. Dai, D. Advanced Passive Silicon Photonic Devices With Asymmetric Waveguide Structures. *Proc. IEEE* **2018**, *106*, 2117–2143. [CrossRef]
6. Kribich, K.; Copperwhite, R.; Barry, H.; Kolodziejczyk, B.; Sabattié, J.-M.; O'Dwyer, K.; MacCraith, B. Novel chemical sensor/biosensor platform based on optical multimode interference (MMI) couplers. *Sens. Actuators B Chem.* **2005**, *107*, 188–192. [CrossRef]

7. Pustelny, T.; Grabka, M. Numerical Investigation of the Photonic-Crystal Fibres with Suspended Core. *Acta Phys. Pol. A* **2009**, *116*, 385–388. [CrossRef]
8. Mazingue, T.; Kribich, R.; Etienne, P.; Moreau, Y. Simulations of refractive index variation in a multimode interference coupler: Application to gas sensing. *Opt. Commun.* **2007**, *278*, 312–316. [CrossRef]
9. Szewczuk, A.; Blahut, M. Multimode Interference Structures of Variable Geometry for Optical Sensor Application. *Acta Phys. Pol. A* **2010**, *118*, 1254–1258. [CrossRef]
10. Masini, G.; Capellini, G.; Witzens, J.; Gunn, C. High-speed, monolithic CMOS receivers at 1550 nm with Ge on Si waveguide photodetectors. In Proceedings of the LEOS 2007-IEEE Lasers and Electro-Optics Society Annual Meeting Conference Proceedings, Lake Buena Vista, FL, USA, 21–25 October 2007; pp. 848–849.
11. Feng, D.; Luff, B.J.; Asghari, M. Recent advances in manufactured silicon photonics integrated circuits. In *Optoelectronic Integrated Circuits XIV*; International Society for Optics and Photonics: Bellingham, WA, USA, 2012; Volume 8265, p. 826507.
12. Pikhtin, N.A.; Slipchenko, S.O.; Sokolova, Z.N.; Tarasov, I.S. Internal optical loss in semiconductor lasers. *Phys. Technol. Semicond.* **2004**, *38*, 360–367. [CrossRef]
13. Madani, A.; Kleinert, M.; Stolarek, D.; Zimmermann, L.; Ma, L.; Schmidt, O.G. Vertical optical ring resonators fully integrated with nanophotonic waveguides on silicon-on-insulator substrates. *Opt. Lett.* **2015**, *40*, 3826–3829. [CrossRef] [PubMed]
14. Frankis, H.C.; Kiani, K.M.; Bonneville, D.B.; Zhang, C.; Norris, S.; Mateman, R.; Leinse, A.; Bassim, N.D.; Knights, A.P.; Bradley, J.D.B. Low-loss TeO2-coated Si3N4 waveguides for application in photonic integrated circuits. *Opt. Express* **2019**, *27*, 12529–12540. [CrossRef]
15. Subramanian, A.Z.; Neutens, P.; Dhakal, A.; Jansen, R.; Claes, T.; Rottenberg, X.; Peyskens, F.; Selvaraja, S.; Helin, P.; Du Bois, B.; et al. Low-loss singlemode PECVD silicon nitride photonic wire waveguides for 532–900 nm wavelength window fabricated within a CMOS pilot line. *IEEE Photonics J.* **2013**, *5*, 2202809. [CrossRef]
16. Huang, Y.; Song, J.; Luo, X.; Liow, T.-Y.; Lo, G.-Q. CMOS compatible monolithic multi-layer Si_3N_4-on-SOI platform for low-loss high performance silicon photonics dense integration. *Opt. Express* **2014**, *22*, 21859–21865. [CrossRef] [PubMed]
17. Romero-García, S.; Merget, F.; Zhong, F.; Finkelstein, H.; Witzens, J. Silicon nitride CMOS-compatible platform for integrated photonics applications at visible wavelengths. *Opt. Express* **2013**, *21*, 14036–14046. [CrossRef]
18. Cirino, G.A.; Barea, L.A.; Von Zuben, A.A.; L'Hermite, H.; Beche, B.; De Sagazan, O.; Frateschi, N.; Brahim, M.-T. Simulation and fabrication of silicon nitride microring resonator by DUV lithography. In Proceedings of the 2016 31st Symposium on Microelectronics Technology and Devices (SBMicro), Belo Horizonte, Brazil, 29 August–3 September 2016; IEEE: Piscataway, NJ, USA, 2016; pp. 1–4.
19. Daldosso, N.; Melchiorri, M.; Riboli, F.; Girardini, M.; Pucker, G.; Crivellari, M.; Bellutti, P.; Lui, A.; Pavesi, L. Comparison among various Si/sub 3/N/sub 4/waveguide geometries grown within a CMOS fabrication pilot line. *J. Lightwave Technol.* **2004**, *22*, 1734–1740. [CrossRef]
20. Gorin, A.; Jaouad, A.; Grondin, E.; Aimez, V.; Charette, P. Fabrication of silicon nitride waveguides for visible-light using PECVD: A study of the effect of plasma frequency on optical properties. *Opt. Express* **2008**, *16*, 13509–13516. [CrossRef]
21. Gondarenko, A.; Levy, J.S.; Lipson, M. High confinement micron-scale silicon nitride high Q ring resonator. *Opt. Express* **2009**, *17*, 11366–11370. [CrossRef] [PubMed]
22. Levy, J.S.; Gondarenko, A.; Foster, M.A.; Turner-Foster, A.C.; Gaeta, A.L.; Lipson, M. CMOS-compatible multiple-wavelength oscillator for on-chip optical interconnects. *Nat. Photonics* **2009**, *4*, 37–40. [CrossRef]
23. Razzari, L.; Duchesne, D.; Ferrera, M.; Morandotti, R.; Chu, S.; Little, E.B.; Moss, D.J. CMOS-compatible integrated optical hyper-parametric oscillator. *Nat. Photonics* **2009**, *4*, 41–45. [CrossRef]
24. Ferdous, F.; Miao, H.; Leaird, D.E.; Srinivasan, K.; Wang, J.; Chen, L.; Varghese, L.T.; Weiner, A.M. Spectral line-by-line pulse shaping of on-chip microresonator frequency combs. *Nat. Photonics* **2011**, *5*, 770–776. [CrossRef]
25. Pfeifle, J.; Weimann, C.; Bach, F.; Riemensberger, J.; Hartinger, K.; Hillerkuss, D.; Jordan, M.; Holtzwarth, R.; Kippenberg, T.J.; Leuthold, J.; et al. *Microresonator-Based Optical Frequency Combs for High-Bitrate WDM Data Transmission*; The Optical Society of America: Washington, DC, USA, 2012; p. OW1C.4.

26. Kippenberg, T.J.; Gaeta, A.L.; Lipson, M.; Gorodetsky, M.L. Dissipative Kerr solitons in optical microresonators. *Science* **2018**, *361*, eaan8083. [CrossRef] [PubMed]
27. Halir, R.; Okawachi, Y.; Levy, J.S.; Foster, M.A.; Lipson, M.; Gaeta, A.L. Ultrabroadband supercontinuum generation in a CMOS-compatible platform. *Opt. Lett.* **2012**, *37*, 1685–1687. [CrossRef] [PubMed]
28. Goykhman, I.; Desiatov, B.; Levy, U. Ultrathin silicon nitride microring resonator for biophotonic applications at 970 nm wavelength. *Appl. Phys. Lett.* **2010**, *97*, 81108. [CrossRef]
29. Voirin, G.; Gehriger, D.; Parriaux, O.M.; Usievich, B.A. Si_3N_4/SiO_2/Si waveguide grating for fluorescent biosensors. In *Integrated Optics Devices III*; International Society for Optics and Photonics: Bellingham, WA, USA, 1999; Volume 3620, pp. 109–116.
30. Cai, H.; Poon, A.W. Optical trapping of microparticles using silicon nitride waveguide junctions and tapered-waveguide junctions on an optofluidic chip. *Lab Chip* **2012**, *12*, 3803–3809. [CrossRef] [PubMed]
31. Tombez, L.; Zhang, E.J.; Orcutt, J.S.; Kamlapurkar, S.; Green, W.M.J. Methane absorption spectroscopy on a silicon photonic chip. *Optica* **2017**, *4*, 1322–1325. [CrossRef]
32. Antonacci, G.; Goyvaerts, J.; Zhao, H.; Baumgartner, B.; Lendl, B.; Baets, R. Ultra-sensitive refractive index gas sensor with functionalized silicon nitride photonic circuits. *arXiv* **2020**, arXiv:2004.04260. [CrossRef]
33. Shaw, M.J.; Guo, J.; Vawter, G.A.; Habermehl, S.; Sullivan, C.T. Fabrication techniques for low-loss silicon nitride waveguides. In *Micromachining Technology for Micro-Optics and Nano-Optics III*; SPIE: Bellingham, WA, USA, 2005; Volume 5720, pp. 109–118.
34. Moreira, R.L. Integrated Optical Delay Line Circuits on a Ultra-Low Loss Planar Waveguide Platform. Ph.D. Thesis, University of California, Santa Barbara, CA, USA, 2016.
35. Shang, H.; Sun, D.; Yu, P.; Wang, B.; Yu, T.; Li, T.; Jiang, H. Investigation for Sidewall Roughness Caused Optical Scattering Loss of Silicon-on-Insulator Waveguides with Confocal Laser Scanning Microscopy. *Coatings* **2020**, *10*, 236. [CrossRef]
36. Witzens, J.; Hochberg, M. Optical detection of target molecule induced aggregation of nanoparticles by means of high-Q resonators. *Opt. Express* **2011**, *19*, 7034–7061. [CrossRef]
37. Neutens, P.; Subramanian, A.; Hasan, M.U.; Chen, C.; Jansen, R.; Claes, T.; Rottenberg, X.; Du Bois, B.; Leyssens, K.; Helin, P.; et al. Characterization of PECVD silicon nitride photonic components at 532 and 900 nm wavelength. *Photonics Eur.* **2014**, *9133*, 91331F.
38. Bagatur'yants, A.A.; Minushev, A.K.; Novoselov, K.P.; Safonov, A.A.; Umanskii, S.Y.; Vladimirov, A.S.; Korkin, A. Atomistic Simulation of Si_3N_4 CVD from Dichlorosilane and NH_3. In *Predictive Simulation of Semiconductor Processing*; Springer: Berlin/Heidelberg, Germany, 2004; pp. 295–355.
39. LIGENTEC SA. Silicon Nitride LIGENTEC. Available online: https://www.ligentec.com/technology-ligentec/siliconnitride-ligentec/ (accessed on 3 April 2019).
40. Bylina, M.S.; Glagolev, S.F.; Kochanovsky, L.N.; Piskunov, V.V. *Measurement of Parameters of Fiber-Optic Linear Paths*; Textbook; Department of Communication Lines SPb GUT by Prof. M.A. Bonch-Bruevich: St. Petersburg, Russian Federation, 2002.
41. Soller, B.J.; Gifford, D.K.; Wolfe, M.S.; Froggatt, M.E. High resolution optical frequency domain reflectometry for characterization of components and assemblies. *Opt. Express* **2005**, *13*, 666–674. [CrossRef]
42. Luke, K.; Okawachi, Y.; Lamont, M.R.E.; Gaeta, A.L.; Lipson, M. Broadband mid-infrared frequency comb generation in a Si_3N_4 microresonator. *Opt. Lett.* **2015**, *40*, 4823–4826. [CrossRef]
43. Lin, P.T.; Singh, V.; Lin, H.-Y.G.; Tiwald, T.; Kimerling, L.C.; Agarwal, A.M. Low-Stress Silicon Nitride Platform for Mid-Infrared Broadband and Monolithically Integrated Microphotonics. *Adv. Opt. Mater.* **2013**, *1*, 732–739. [CrossRef]
44. Shao, Z.; Chen, Y.; Chen, H.; Zhang, Y.; Zhang, F.; Jian, J.; Fan, Z.; Liu, L.; Yang, C.; Zhou, L.; et al. Ultra-low temperature silicon nitride photonic integration platform. *Opt. Express* **2016**, *24*, 1865–1872. [CrossRef]

Publisher's Note: MDPI stays neutral with regard to jurisdictional claims in published maps and institutional affiliations.

© 2020 by the authors. Licensee MDPI, Basel, Switzerland. This article is an open access article distributed under the terms and conditions of the Creative Commons Attribution (CC BY) license (http://creativecommons.org/licenses/by/4.0/).